# *Chapter 6.7*

# 3D imaging, colour and specularity of an Egyptian Scarab

Lindsay MacDonald & Mona Hess

The analysis of Egyptian gold items shows evidence for polychrome effects, using not only coloured materials but also several gold alloys with different copper and silver contents. The latter necessitate an effective method for analysing the colours present in the object – knowing that in some alloys atmospheric corrosion may alter the surface, and 'hide' the original colour.

The physical surface of an artefact is influenced by decorative techniques, evidenced by the presence of tool marks, and by wear-marks, giving indications about the object's intended function and possible reuse. Scientific visual analysis requires images of high quality, at different scales and depths. For this reason, we wished to investigate the capability of 3D image acquisition to represent the colour and surface detail of materials used in the production of Egyptian gold jewellery.

The object selected for this pilot study is a small scarab of engraved steatite set in a gold band, from the UCL Petrie Museum of Egyptian Archaeology (UC11365, Fig. 6.24). Dated to the Late Middle Kingdom (1850–1750 BC), it is inscribed in hieroglyphs on the underside with the personal name and title 'estate overseer of the granary Iufseneb' within the scroll border. The hole of 2.8 mm diameter drilled through the centre suggests that it may have been suspended on a cord worn around the wrist or neck, or fitted onto a metal rod in a ring mounting, and used as an administrative seal in clay tablets or in wax on papyrus.

**3D digitization**

Different methods of 3D acquisition were studied for their ability to represent the original colours and surface details for visual inspection of toolmarks and other material properties. The scarab poses particular challenges for imaging due to its characteristics: a small object, with finely engraved inscription, the back is curved and polished to a semi-gloss finish, and the encircling chased gold band has a high metallic specularity.

*Photogrammetric method*

The scarab was placed on a rigid black card, onto which were affixed a number of retro-reflective targets for geometric camera calibration (Fig. 6.25). Around 80 images were taken using a fixed Nikon D3200 camera with 105 mm macro lens, from various angles by rotating the tray, and by turning the scarab onto its side. Flash lighting was diffused by soft boxes and reflectors pointed towards the ceiling. The image set was processed with an in-house software pipeline at UCL, enabling a dense and accurate 3D point cloud to be generated (Ahmadabadian et al. 2013). After geometrically correcting ('undistorting') the images, by estimating parameters from the camera's chip size and focal length, the approximate 3D coordinates were extracted from the images. A photogrammetric bundle adjustment with the relative orientation parameters of each camera position enabled the scale factor to be estimated and then applied to the camera locations and 3D coordinates of the scarab surface. These data were input into the processing software to generate a dense point cloud.

As the scarab needed to be repositioned during acquisition in order to obtain images of the whole object, each 'scene' was reconstructed separately, then cleaned and fused together during post-processing. The resulting 3D surface geometry shows a greater variance, or level of noise, than that of a laser scanner (compare Fig. 6.27 middle to Fig. 6.28 middle). However, this method of photogrammetric imaging, including a colour chart and subsequent calibration, enables the acquisition of accurate colour data, which is essential for cultural heritage applications. If a mesh is reconstructed from the point cloud, the colour texture

**Figure 6.24.** *Six views of scarab UC11365, Petrie Museum. Dimensions (in mm) 26.7 (W) × 18.6 (H) × 11.4 (D). Photographed with a Nikon D200 camera with Nikkor 200 mm macro lens, illuminated by 16 flashlights in a circular ring.*

**Figure 6.25.** *Photogrammetric imaging setup with scarab UC11365 on target board.*

obtained from the imagery can then be reprojected onto the surface giving a high resolution rendering even on a lower resolution geometric structure.

*3D colour laser scanning*

A 3D colour laser scanner at UCL has been used extensively for digitization of museum objects, and for traceable and repeatable production of metric surface models. It delivers 3D RGB point data at a sampling interval of 0.1 mm (100 μm) with an absolute accuracy of 0.025 mm (25 μm) over the object surface (Hess & Robson 2010). Twenty-six separate scans of the scarab were made, with the object turned to many different orientations to ensure that all surfaces were captured. The corresponding point clouds were merged to produce a 3D representation with *c.* 402,000 points.

*Photometric stereo*

The dome imaging system at UCL enables sets of images of an object to be taken with illumination from different directions (Fig. 6.26). A hemisphere of 104 cm diameter is fitted with 64 flash lights, and calibrated so that the geometric centroid coordinates of every light source are known to within 3 mm (MacDonald et al. 2015). A Nikon D200 digital camera at the 'north pole' captures a series of 64 colour images, each illuminated from a different direction and all in pixel register. This enables the object to be visualized from the fixed viewing angle of the camera, i.e. vertically from above, for many different angles of incident light. Image sets captured by the system can be visualized for a directional light source by the polynomial texture mapping (PTM) technique, which has numerous applications in archaeology and cultural heritage (Earl et al. 2010).

Six sets of images from the UCL dome were used to reconstruct the 3D surface of the scarab by

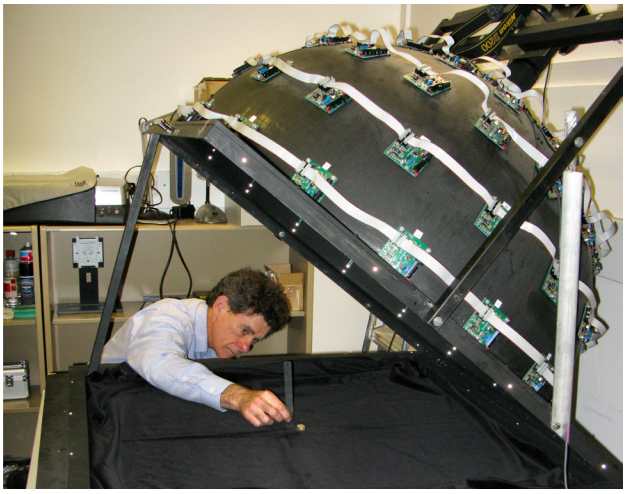

**Figure 6.26.** *Positioning scarab UC11365 on the baseboard of the UCL dome.*

the photometric stereo method (MacDonald & Robson 2010), by determining the surface normal vector at each pixel then integrating the set into a consistent surface. An adaptive method was developed to find an optimal subset of intensities from all 64 candidates at each pixel, by sorting them into order and selecting a range between the shadow and specular regions, followed by regression over this subset for an accurate estimate of the normal vector (see below). The height field was reconstructed as a digital terrain map by projecting the surface gradients onto Fourier basis functions to ensure integrability (MacDonald 2015), then exported as a point cloud for 3D visualization.

**Evaluation of 3D reconstruction methods**

The various 3D representations were evaluated for visibility of toolmarks and other material treatments. The 3D coloured point clouds produced by the models were rendered for display.

The photogrammetric method showed realistic colour and significant detail (Fig. 6.27), with a resolution of approximately 20 pixels/mm (50 μm sampling). The overall geometry was accurate but was compromised by holes in the 3D point cloud from missing data due to specular reflection from the gold during the acquisition process. There was also a noticeable level of surface noise in the reconstruction.

The 3D colour laser scanner produced good geometric accuracy, but the rendition of surface detail was poor (Fig. 6.28). Even though the scanner was expected to show sufficient details with a sampling distance of 100 μm, i.e. a spatial resolution of 10 points/mm, it did not meet the expectation, and revealed less detail than shown by magnification with a hand lens. The finest surface feature that can be wrought on an artefact by a craftsman with manual techniques is approximately 40 μm in width, to capture which the scanner should be

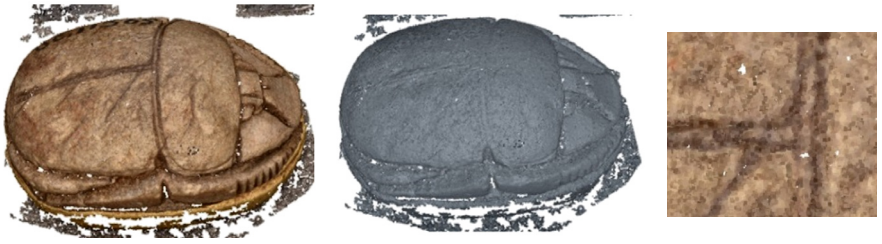

**Figure 6.27.** *(left) Photogrammetric reconstruction; (centre) without colour. Although the colour was close to original object, the method produced a significant quantity of surface noise and holes in the 3D point cloud. (right) Detail of scarab top, showing erroneous cut by craftsman.*

**Figure 6.28.** *3D point cloud generated by the colour laser scanner, showing the redness caused by non-optimal laser wavelengths.*

**Figure 6.29.** *3D reconstruction from photometric normals produced a very dense point cloud with outstanding detail of surface features.*

able to resolve 20 μm, i.e. 50 pixels/mm or 1250 pixels per inch (MacDonald 2010). Moreover, the rendering of surface colour shows less fidelity to real colour than with a camera, because the monochromatic sampling of the reflectance spectrum by the three lasers leads to severe metamerism (MacDonald 2011).

The photometric stereo reconstruction in 3D was accurate over the rounded back of the scarab for a range of ±45° from the vertical (Fig. 6.29), and gave excellent rendering of fine detail, especially helpful for reading the hieroglyphs on the underside. Comparison of the 3D point cloud produced by the photometric stereo technique with the reference point cloud from the laser scanner (Fig. 6.30) shows that the mean error was less than 0.25 mm, but around the sides and the gold band, the errors were larger in the range 0.4 to 0.7 mm.

The results of the qualitative evaluation of the three reconstruction methods are summarized in Table 6.8. The laser scanner gave results that were excellent in terms of geometric accuracy, because of the precision of its coordinate measuring machine (CMM), but its results were inferior in both colour and spatial resolution to the other techniques which derived 3D from sets of photographic images (MacDonald et al. 2014). For all methods the time required to set up and digitize the object was typically about an hour, followed by a day or more of operator time and/or computing time to process the data to produce the final 3D representation. In terms of portability, the photogrammetric method was best by far, because it required only a camera and aboard with targets affixed, whereas the photometric stereo method relied on the dome structure to provide the camera support and multiple sources of illumination.

*Colour of gold*

There is nothing absolute about the colour of any object surface: it changes continually with illumination and orientation. Colorimetry specifies the colour as the product of the illuminating power by the reflectance factor of the surface by the sensitivity of the observer, integrated over all wavelengths of the visible spectrum. This is the basis of the ubiquitous CIE system (Colorimetry 2004), but it relies on the assumption that the surface is perfectly matte so every point reflects the incident light equally in all directions, i.e. that it is Lambertian. In fact, almost

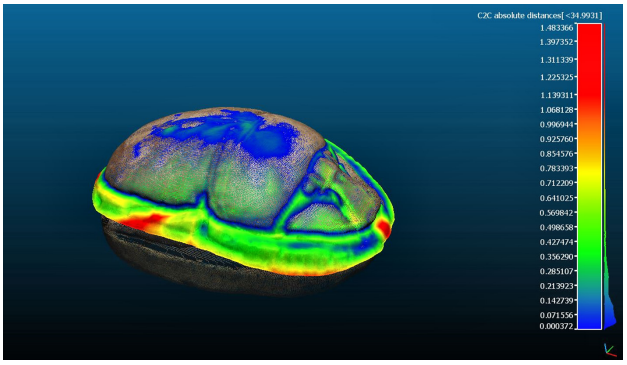


**Figure 6.30.** *Comparison of point cloud from photometric stereo reconstruction with point cloud from laser scanner, using the CloudCompare utility.*

all real materials exhibit some angular dependence in the way they reflect light, and this behaviour must be taken into account when modelling appearance, by adding a gloss component to the underlying diffuse colour. The added light may appear as a sheen over the surface or as localized specular highlights, but its effect is to modulate the lightness and thereby to change the apparent colour.

This is especially true of gold, which combines glitter, specularity and sheen over a wide range of angles to give it a uniquely lustrous quality that sets it apart from ordinary materials. To specify the colour of gold only by a single colorimetric triplet, or even by a single reflectance spectrum, would be dull indeed. As a demonstration, the gold band around the scarab was measured with an Xrite i1Pro spectrophotometer. The instrument illuminates the sample at 45° and analyses the radiation reflected perpendicular to the surface, averaging the rays over a circular beam area of diameter 3.5 mm. The spectral reflectance distributions from 10 successive measurements are shown in Figure 6.31. The characteristic rise in reflectance factor between 480 and 540 nm corresponds to an energy band at 2.3 eV in pure gold where free electrons in the d-band can make the transition to unoccupied states in the conduction band (Saeger & Rodies 1977).

It is evident in the set of measurements that, although the shape of the curve remains the same, the magnitude of the reflectance varies by a factor of 1.5. This can be explained by the measurement geometry

**Table 6.8.** *Qualitative comparison of 3D representations.*

| Technology | Colour | Geometry | Resolution | Cost | Portability |
|---|---|---|---|---|---|
| Photogrammetric method | Good | Good | High | Low | Good |
| 3D colour laser scanning | Poor | Excellent | Medium | High | Impossible |
| Photometric stereo | Good | Poor | High | Medium | Poor |

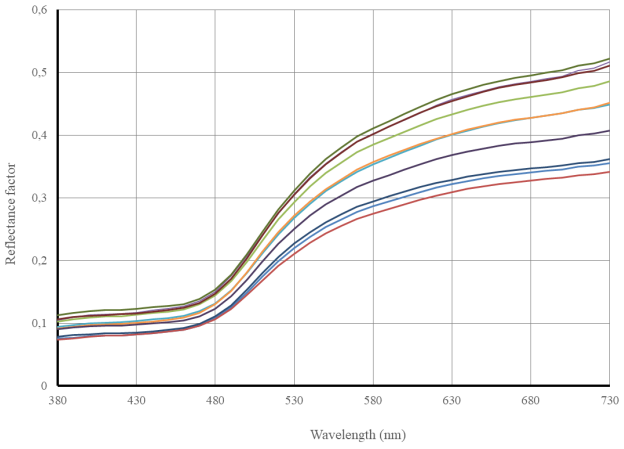


**Figure 6.31.** *(top left) Measurement of gold band on scarab; (bottom left) underside of instrument, showing measuring aperture; (right) set of reflectance spectra.*

of the instrument, which is designed for measurement of flat surfaces, such as prints on paper, which may or may not be glossy. The 45° angle of incident light and 0° angle of view for the sensor ensure that the specular component of reflection is avoided as far as possible. But when the instrument is removed and then brought back each time with the aperture in a slightly different position over the relief surface of the gold, a different distribution of scattered light reaches the sensor and hence the reading changes.

The majority of variation in the measured colorimetric values is in the luminance, not the colour: in CIE 1931 chromaticity coordinates the mean and standard deviation in $x,y,Y$ are [0.4076±0.0013, 0.4166±0.0012, 30.19±4.39] and in $L^*a^*b^*$ the corresponding range is [61.65±3.83, 3.28±0.46, 36.26±1.95]. The latter are plotted in Figure 6.32, showing lightness ($L^*$) vs chroma ($C^*$) and the chromatic plane $a^*b^*$. The standard D65 daylight illuminant was used for computation of the $L^*a^*b^*$ values.

*Specularity of gold*

The scarab was photographed under the illumination dome in six different orientations, with a Nikkor 200 mm macro lens giving a spatial resolution of approximately 66 pixels/mm, i.e. each pixel representing 16 μm on the object surface.

All 64 images in the set from the dome are in pixel register, so each pixel may be regarded as a vector of 64 intensity values, each representing the amplitude of the light reflected from that point on the surface toward the camera for the angle of incidence corresponding to the position of the lamp. The distribution of these 64 intensity values gives an indication of the type of surface (Fig. 6.33).

A notable characteristic of gold, and indeed of all shiny materials, is that it reflects strongly in the specular direction. So in the pixel vector a few intensity values are much larger than the others, corresponding to positions where the surface normal is close to the bisector of the angle between the illumination vector (toward the light) and the view vector (toward the camera). This results in images with high dynamic range where a few pixels may be 100 times greater in value than the majority. In the dome, images are captured and processed as linear intensities with 16-bits per channel (range 0–65535), setting the lens aperture

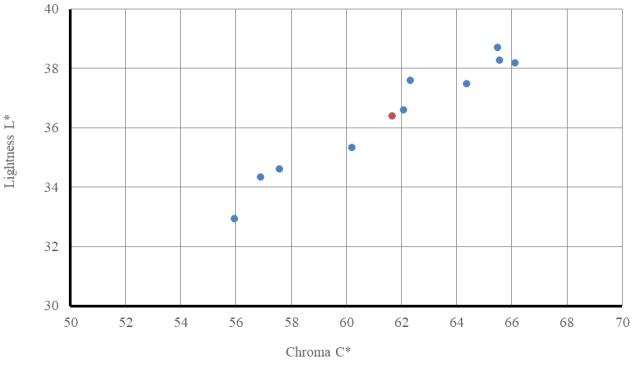


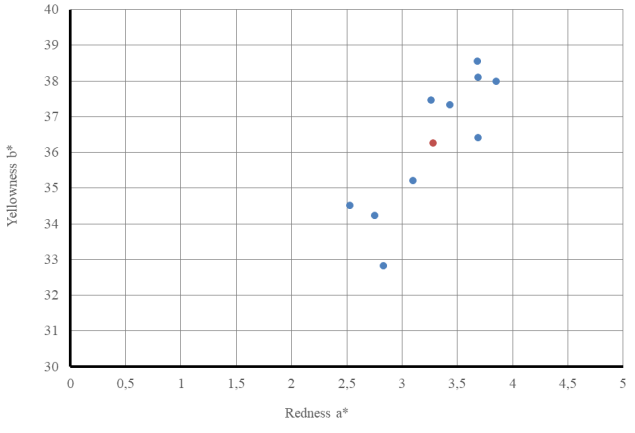


**Figure 6.32.** *Colorimetric coordinates of 10 measurements at different positions on the gold band around the scarab (mean shown in red).*

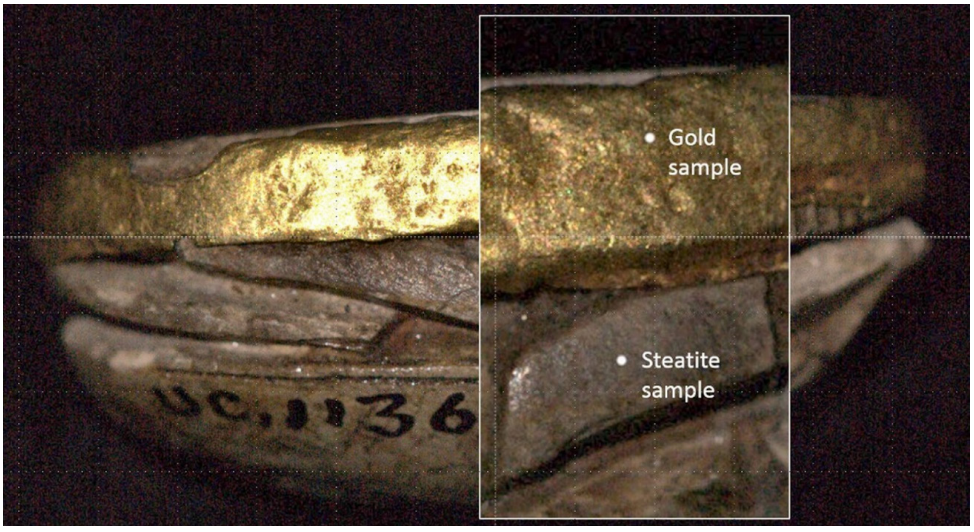


**Figure 6.33.** *Image of left side of scarab, with enlarged detail showing sampling locations for gold and steatite.*

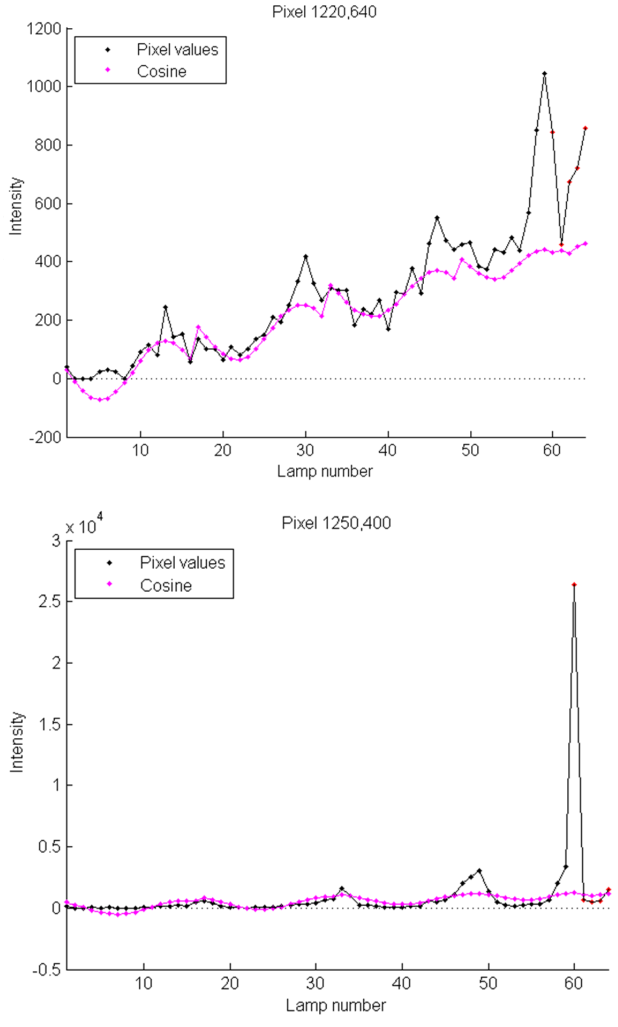


**Figure 6.34.** *Intensity distributions from 64 lamps for a single pixel for: (top) steatite; (above) gold; sampled at positions shown in Figure 6.33.*

to f/8 to avoid over-exposure. Figure 6.34 (right) shows the intensity distribution for a single pixel on the gold band. The maximum value is over 26,000 and seven are in the range 1000–4000, but most others are less than 300. The magenta curve shows what the intensities would be for a perfectly matte (Lambertian) surface with the same albedo and normal angle. It is clear that the specular peaks are much greater in intensity than the cosine, but all other values are lower. Thus, the metallic gold surface is generally darker than the diffuse equivalent, except for a few bright highlights.

The processing method is to identify from the sorted intensity distribution of a 3 × 3 pixel neighbourhood a limited range of values between the shadow and specular regions, which are taken to be representative of the non-specular 'body colour' of the object. Then, using the principle of 'shape from shading', a regression is performed on the corresponding lamp vectors to estimate the most probable direction of the surface normal vector at that pixel (MacDonald 2014). The albedo is the magnitude of the normal vector, and its appearance is surprisingly dark (Fig. 6.35 left). The normal vectors are represented in Figure 6.35 (right) by the conventional false-colour coding scheme with X components in red, Y in green and Z in blue.

The second stage of processing is to determine the specular vector at each pixel, i.e. the direction of maximum specular reflectance. First, the specular quotient (ratio) is calculated between the actual intensity value and the diffuse component for each lamp. This would be the black value divided by the magenta value for each of the 64 points in Figure 6.35. For semi-matte surfaces the quotient values are typically in the range 0.5 to 2.5, but for high gloss and shiny metallic surfaces they may be very large. In this case the gold band has a bright lustre rather than a brilliant shine,

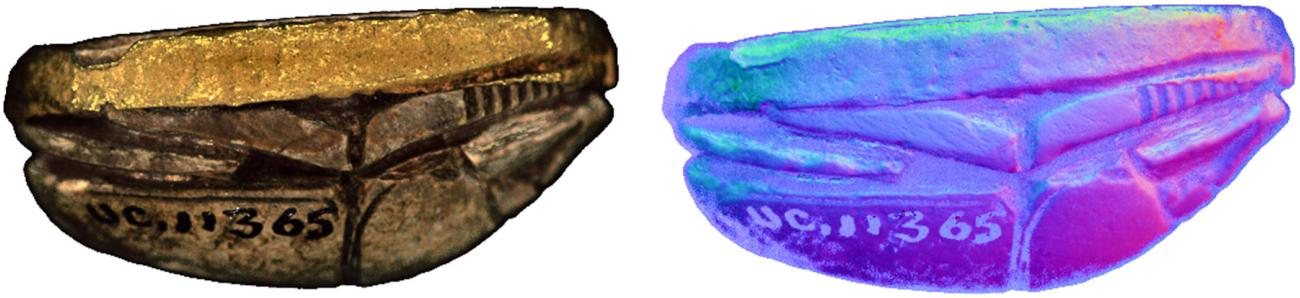

**Figure 6.35.** *Image components derived from processing the original set of 64 images: (left) albedo, (right) normals.*

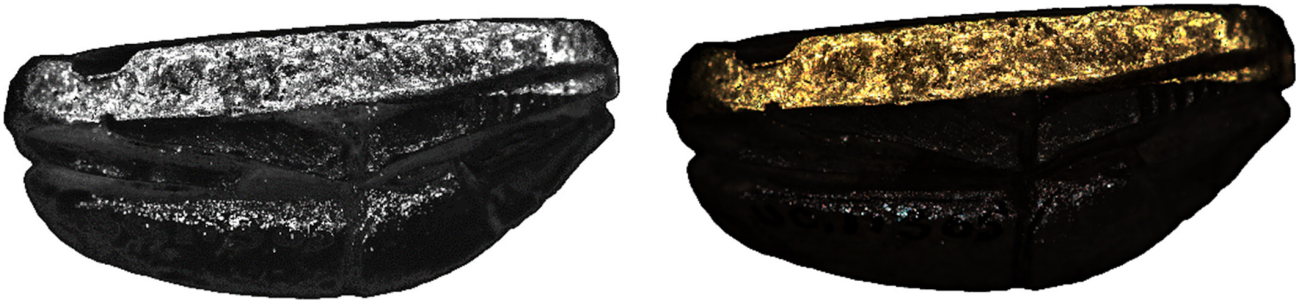

**Figure 6.36.** *Image components: (left) specular quotient, (right) specular colour.*

with a maximum specular quotient value of 67.5 and mean of 11.2 with standard deviation 2.7 (Fig. 6.36).

One might suppose that the specular angle should be exactly double that of the normal, as it would be for a perfect mirror surface, but in fact there is a great deal of variation. This is caused by granularity of the metallic gold and surface imperfections, such as scratches and dust, which cause perturbations in the direction of the strongest reflectance. The scatter is clear when the specular angle relative to the Z-axis is plotted against the normal angle for 10 000 points randomly selected throughout the gold band region of the image (Fig. 6.36 left). Instead of lying along the line of slope 2, they are spread over a wide range of angles, both greater than and less than the normal angle. The horizontal lines of red dots in the figure are computational artefacts, where the specular vector lies exactly toward the lamp, in this case in the second tier of the dome with an incident angle of approximately 26°.

The specular colour at each pixel is computed from the colours of the selected specular values, using the same weighting factor derived from the specular quotient. The result is shown in Figure 6.36 (right) and it is apparent that the specular colour of the gold band is lighter and less saturated than the albedo colour in Figure 6.36 (left). The relationship of the angles can be explored by plotting corresponding values for a random selection of 10,000 points throughout the area of the gold band. In the 3D scatter plot of Figure 6.37 (right) the albedo colours are shown as black dots and the specular colours as red dots in a normalized R,G,B cube. Also shown are lines representing the first principal component of each cluster of points, which tend in different directions. The albedo (body colour) is darker, whereas the specular colour is lighter and closer to the neutral axis, although the specular data is more scattered. Both are below neutral on the blue axis, meaning that both are yellowish. The two vectors in RGB colour space (denoted by the red and black lines in Fig. 6.37 right) may be considered as equivalent to the interface and body colours identified by Shafer in his proposal for a dichromatic model of reflection from a material surface (Shafer 1985).

The angular distribution of the specular quotient around the specular peak has been found for a variety of materials to be modelled well by a modified Lorentzian function, which takes the form of a curved peak plus a linear flank (MacDonald 2014). The parameters of the curve are determined for each pixel by fitting the distribution of specular quotient values in the polar plane (Fig. 6.38 left). The function generated by the mean parameter values over all pixels in the gold band has an angular width at half-maximum amplitude of 17.5° (Fig. 6.38 right). This is in good

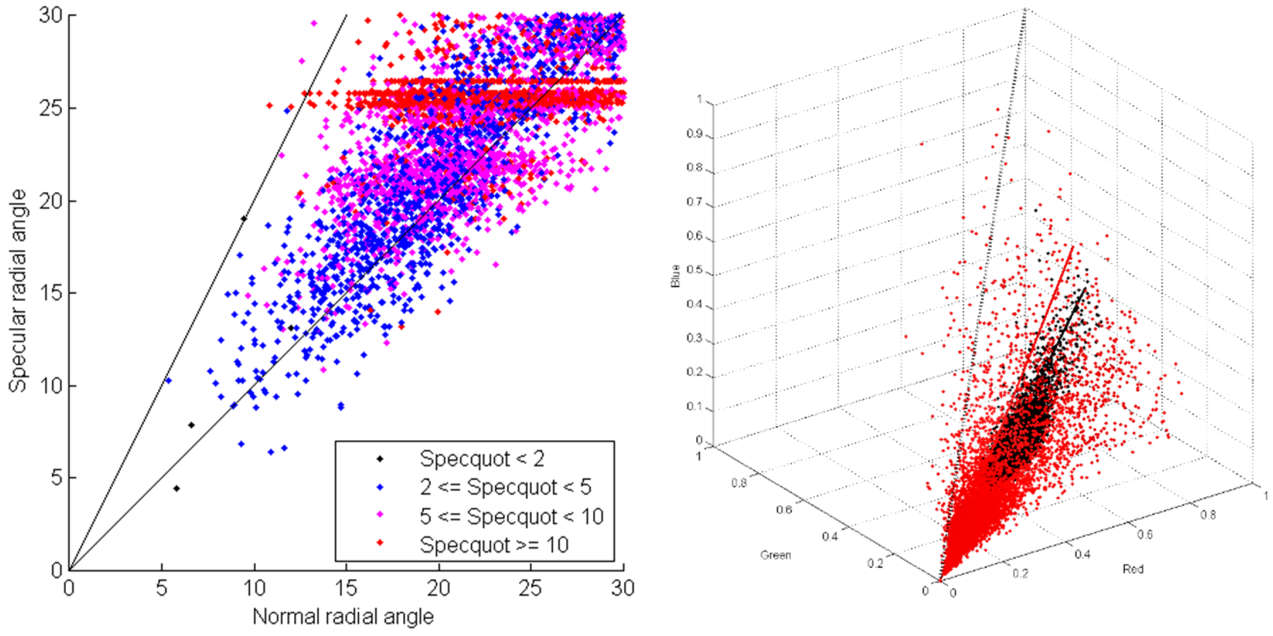


**Figure 6.37.** *(left) Scatter plot of specular vector angle vs normal vector angle; (right) specular vs albedo colours for 10,000 random points in gold band.*

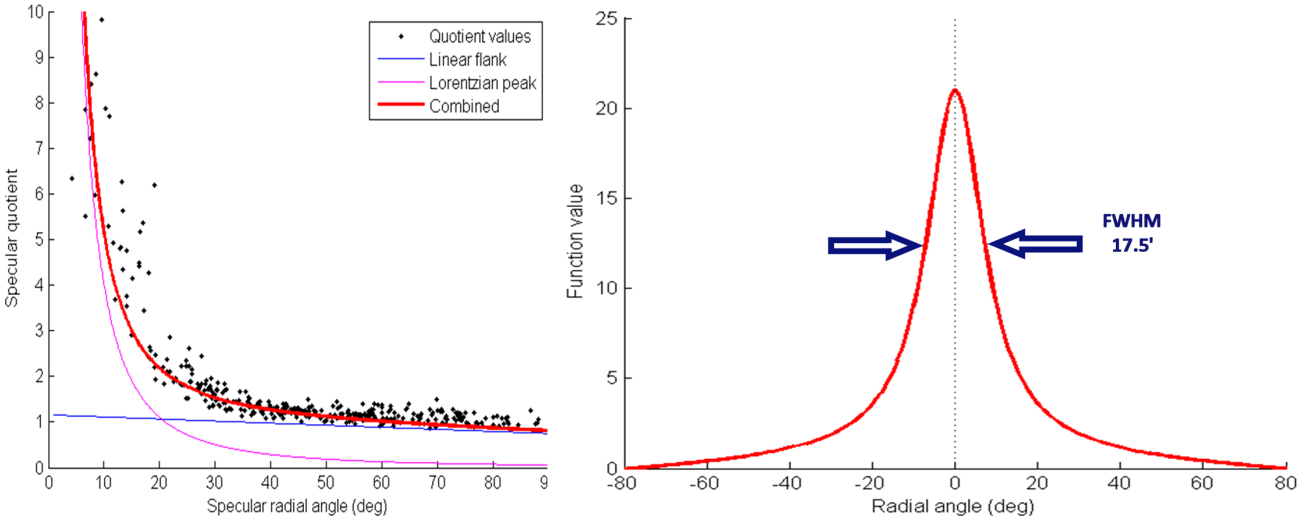


**Figure 6.38.** *(left) Fitting of flank and Lorentzian function through specular quotient values; (right) function generated with mean of parameter values.*

agreement with values found in other studies of gold (Lee at al. 2006). Note that the specular reflection is not restricted mirror-like to the specular peak angle, but extends over a wide range of angles, which gives gold its characteristic lustre. Without this broad flank in the specular reflectance distribution, the rendering of gold would be darker with scattered pinpoint highlights and would not be realistic.

The complete model for rendering images under a single light source adds the diffuse and specular terms. This gives images that are realistic in appearance and a good match to actual photographs. Figure 6.39 juxtaposes the actual photographic image taken in the dome illuminated by lamp 60 (high up in the dome to the right) with the rendered image illuminated from the same angle. Although not identical, the two are

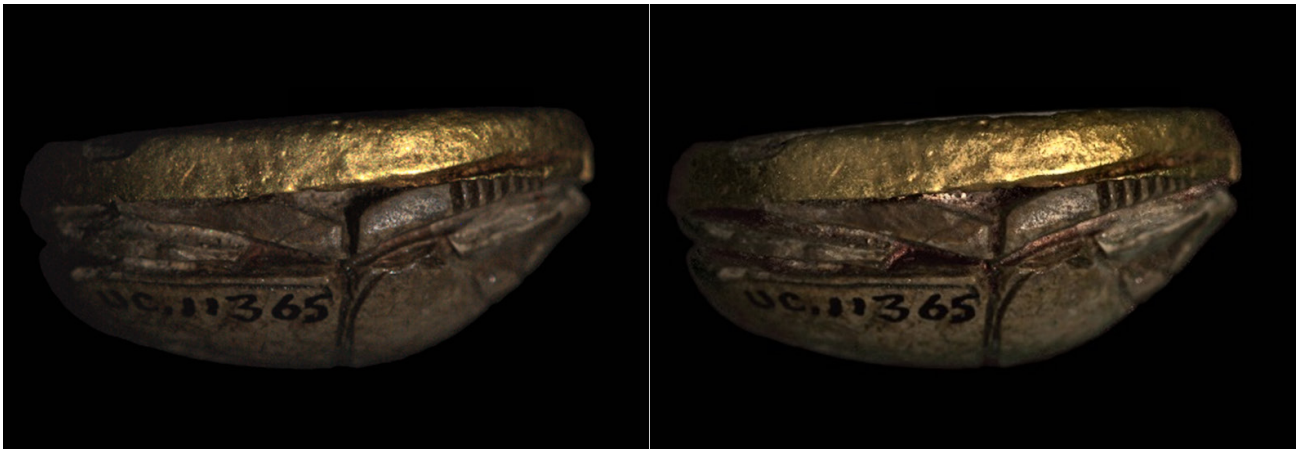

**Figure 6.39.** *(left) Original photograph and (right) rendered image, both illuminated from same hemisphere coordinates as original lamp.*

similar in terms of the overall tonality and distribution of highlights. Because the model is based on a continuous function of angle, images can be rendered for a virtual light source at any position in the hemisphere.

Thus, the colour of gold can be represented as a sum of two components: a dark reddish-yellow 'body colour', the albedo corresponding to the diffuse reflectance from the material, plus a bright yellowish highlight with a broad angular distribution around the specular peak. Multiple reflections from facets on the surface may cause the spectrum of the reflected light to be multiplied and hence to appear darker and more saturated. When the object is diffusely illuminated, with incident light from many directions, the characteristic golden radiance suffuses the whole surface and brings it to life.

**Acknowledgements**

This study was facilitated by the European COST Action TD1201 Colour and Space in Cultural Heritage (COSCH). Some of these results were presented previously in a conference paper (MacDonald et al. 2014). Thanks especially to colleagues in the 3DIMPact research group Stuart Robson and Ali Hosseininaveh Ahmadabadian, who carried out the 3D laser scanning and the point cloud processing and the photogrammetric reconstruction (Ahmadabadian et al. 2013).

**References**

For references see pp.185–91 at the end of this chapter.

**References (for complete Chapter 6)**


Abdrabou, A., El Hadidi, N.M.N., Hamed, S. & Abdallah, M., 2018. Multidisciplinary approach for the investigation and analysis of a gilded wooden bed of King Tutankhamun. *Journal of Archaeological Science: Reports* 21, 553–64.

Abramowitz, M., 2003, *Microscope*. Basics and Beyond Series 1, revised edition. Melville, NY: Olympus America Inc.

Adriaens A. & Dowsett, M.G., 2004. Electron microscopy and its role in cultural heritage studies, in *Comprehensive Analytical Chemistry* 42, eds. K. Janssens & R. Van Grieken. Amsterdam: Elsevier B.V., 73-128.

Adrimi-Sismani, V., Guerra, M.F. & Walter, P., 2009. La tombe mycénienne de Kazanaki (Volos) et le mythe de la Toison d'or. *ArcheoSciences* 33, 135–41.

Ahmadabadian, A.H., Robson, S., Boehm, J. & Shortis, M., 2013. Image Selection in photogrammetric multi-view stereo methods for 3D reconstruction, in V*ideometrics, Range Imaging, and Applications XII*, eds. F. Remondino, M.R. Shortis, J. Beyerer & F. Puente León. SPIE Conference Proceedings 8791. The International Society for Optical Engineering, Article 879107.

Alvarez, M.G., Fernández, S.A. & Galvele, J.R., 2002. Effect of temperature on transgranular and intergranular stress corrosion crack velocity of Ag-Au alloys. *Corrosion Science* 44, 2831–40.

Andrews, C., 1990. *Ancient Egyptian jewellery*. London: British Museum Publications.

Angelini, E., Grassini, S. & Tusa, S., 2013. Underwater corrosion of metallic heritage artifacts, in *Corrosion and conservation of cultural heritage metallic artefacts*, eds. Dillmann, P., Watkinson, D., Angelini, E. & A. Adriaens. European Federation of Corrosion Publications 65. Cambridge: Woodhead Publishing Limited, 236–59.

Aruz, J., 2008. Falcon with prey & Lid with falcons in *Beyond Babylon. Art Trade and Diplomacy in the Second Millennium* BC, eds. J. Aruz. K. Benzel & J. M. Evans. New York / New Haven / London: The Metropolitan Museum of Art / Yale University Press, 88–9.

Assaf, F.H., Zaky, A.M. & El-Rehim, S.S.A., 2002. Cyclic voltammetric studies of the electrochemical behaviour of copper-silver alloys in NaOH solution. *Applied Surface Science* 187, 18–27.

Barham, E., 2007. Controlled lifting and X-radiography of gold threads from ancient archaeological textiles, in *X-Radiography of Textiles, Dress and Related Objects*, eds. S. O'Connor & M.M. Brooks. Oxford: Butterworth-Heinemann, 302–6.

Barreiros, M.A. & Marcelo, T., 2014. Estudos por SEM-EDS de torques, braceletes e arrecadas, in *A ourivesaria pré-histórica do Ocidente Peninsular Atlântico: compreender para conservar*, eds. M.F. Guerra & I. Tissot. Lisbon: AuCORRE, 59–62.

Bass, G.F., 1986. A Bronze Age Shipwreck at Ulu Burun (Kaş): 1984 Campaign. *American Journal of Archaeology* 90(3), 269–96.

Bass, M. (ed.), 2010. *Handbook of Optics I*, 3rd edition. The McGraw-Hill Companies, Inc.

Bastidas, D.M., Cano, E., González, A.G., Fajardo, S., Lleras-Pérez, R., Campo-Montero, E., Belzunce-Varela, F.J. & Bastidas, J.M., 2008. An XPS study of tarnishing of a gold mask from a pre-Columbian culture. *Corrosion Science* 50, 1785–8.

Beckhoff, B., Kanngießer, B., Langhoff, N., Wedell, R. & Wolff, H., 2007. *Handbook of Practical X-Ray Fluorescence Analysis*. Berlin Heidelberg: Springer-Verlag.

Bianucci, R., Habicht, M.E., Buckley, S., Fletcher, J., Seiler, R., Öhrström, L.M., Vassilika, E., Böni, T., & Rühli, F. J., 2015. Shedding New Light on the 18th Dynasty Mummies of the Royal Architect Kha and His Spouse Merit. *PloS one* 10(7), e0131916.

Binder, S., 2008. *The Gold of Honour in New Kingdom Egypt*. Oxford: Aris & Phillips Ltd.

Blaber, M.G., Ford, M.J. & Cortie, M.B., 2010. The Physics and Optical Properties of Gold, in *Gold: science and applications*, eds. C. Corti & R. Holliday. CRC Press, Taylor and Francis Group, 13–30.

von Bohlen, A., Hergenroder, R., Sternemann, C., Paulus, M., Radtke, M. & Riesemeier, H., 2005. Wavelength dispersive synchrotron microprobe used for material analysis. *Instrumentation Science & Technology* 33(2), 137–50.

Boone, M.N., Garrevoet, J., Tack, P., Scharf, O., Cormode, D.P., Van Loo, D., Pauwels, E., Dierick, M., Vincze, L. & Van Hoorebeke, L., 2014. High spectral and spatial resolution X-ray transmission radiography and tomography using a Color X-ray Camera. *Nuclear Instruments & Methods in Physics Research A* 735, 644–8.

Borel, T., 1995. La radiographie des objets d'art. *Techné* 2, 146–57.

Bouchard, J.F. & Guerra, M.F., 2009. Archéologie précolombienne et analyses scientifiques. La figurine d'El Angel, une œuvre composite d'orfèvrerie de la culture La Tolita Tumaco (Équateur-Colombie). *ArcheoSciences* 33, 273–9.

Brunetti, B.G., Cartechini, L., Miliani, C. & Sgamellotti, A., 2013. Metal Nanoparticles in Glass: Lustre, in *Modern Methods for Analysing Archaeological and Historical Glass*, ed. K. Janssens. John Wiley & Sons, Ltd., 583–608.

Burgess, S., Li, X. & Holland, J., 2013. High spatial resolution energy dispersive X-ray spectrometry in the SEM and the detection of light elements including lithium. *Microscopy and Analysis* 27(4), S8–S13.

Campbell, J.L., Boyd, N.I., Grassi, N., Bonnick, P. & Maxwell, J.A., 2010. The Guelph PIXE software package IV. *Nuclear Instruments and Methods in Physics Research B* 268, 3356–63.

Campo, E., Vera, E., Göllner, J., Ortiz, C.A. & Lleras, R., 2009. Degradación de piezas arqueológicas "Colección Calima" Museo del Oro. *Suplemento de la Revista Latinoamericana de Metalurgia y Materiales* S1(2), 657–61.

Carvalho, O., Soares, D., Fonseca, A. & Silva, F.S., 2009. Tarnish and corrosion evaluation of a blue-gold based alloy. *Materials and Corrosion* 60, 355–9.

Casali, F., 2006. X-ray and Neutron Digital Radiography and Computed Tomography for Cultural Heritage, in *Physical Techniques in the Study of Art, Archaeology*

*and Cultural Heritage I*, eds. D. Creagh & D. Bradley. Amsterdam: Elsevier B.V., 41–123.

Cason, C., Pezzato, L., Breda, M., Furlan, F. & Dabalà, M., 2015. Effect of microstructure and residual stresses, generated from different annealing and deformation processes, on the corrosion and mechanical properties of gold welding alloy wires. *Gold Bulletin* 48, 135–45.

Champollion, J.-F., 1827. *Notice descriptive des monuments égyptiens du musée Charles X*. Paris: Imprimerie de Crapelet

Chana, M.S. & Kuhn, A.T., 1984. A critique of the Tuccillo-Nielsen wheel method for tarnish testing of dental alloys. *Journal of Dentistry* 12, 314–8.

Colorimetry, 2004. *CIE 15 technical report*, 3rd edition. Vienna: International Commission on Illumination.

Corregidor, V., Alves, L.C. & Cruz, J., 2013. Analysis of surface stains on modern gold coins. *Nuclear Instruments and Methods in Physics Research B* 306, 232–5.

Corso, P.P., German, R.M. & Simmons, H.D., 1985a. Corrosion evaluation of gold-based dental alloys. *Journal of Dental Research* 64, 854–9.

Corso, P.P., German, R.M. & Simmons, H.D., 1985b. Tarnish evaluation of gold-based dental alloys. *Journal of Dental Research* 64, 848–53.

Costa, V., 2001. The deterioration of silver alloys and some aspects of their conservation. *Studies in Conservation* 46(1), 18–34.

Courty, C., Matthieu, H.J. & Landolt, D., 1991. Tarnishing of Au-Ag-Cu alloy studied by Auger electron spectroscopy and coulometry. *Materials and Corrosion* 42, 288–95.

Croft, W.J., 2006. *Under the Microscope: A Brief History of Microscopy*. Singapore: World Scientific Publishing Co. Pte. Ltd.

Curto, S. & Mancini, M., 1968. News of Kha' and Meryt. *The Journal of Egyptian Archaeology* 54, 77–81.

Degrigny, C., Tanguy, E., Le Gall, R., Zafiropulos, V. & Marakis, G., 2003. Laser cleaning of tarnished silver and copper threads in museum textiles. *Journal of Cultural Heritage* 4, 152–6.

Dowben, P.A., Miller, A.H. & Vook, R.W., 1987. Surface segregation from gold alloys. *Gold Bulletin* 20, 54–65.

Duczko, W., 1985. *The filigree and granulation work of the Viking Period. An analysis of the material from Björkö.* Birka V. Stockholm: Kungl. Vitterhets Historie och Antikvitets Akademien

Dugmore, J.M.M. & DesForges, C.D., 1979. Stress corrosion in gold alloys. *Gold Bulletin* 4, 140–4.

Earl, G., Martinez, K. & Malzbender, T., 2010. Archaeological applications of polynomial texture mapping: analysis, conservation and representation. *Journal of Archaeological Science* 37(8), 2040–50.

Elechiguerra, J.L., Larios-Lopez, L., Liu, C., Garcia-Gutierrez, D., Camacho-Bragado, A. & Yacaman, M.J., 2005. Corrosion at the nanoscale: the case of silver nanowires and nanoparticles. *Chemistry of Materials* 17, 6042–52.

Fearon, E., Sato, T., Wellburn, D., Watkins, K.G. & Dearden, G., 2007. Thermal effects of substrate materials used in the laser curing of particulate silver inks. *Laser Assisted Net Shape Engineering* 5, 379–90

Festa, G., Minniti, T., Arcidiacono, L., Borla, M., Di Martino, D., Facchetti, F., Ferraris, E., Turina, V., Kockelmann, W., Kelleher, J., Senesi, R., Greco, C. & Andreani, C., 2018. Egyptian Grave Goods of Kha and Merit Studied by Neutron and Gamma Techniques. *Angewandte Chemie* 57(25), 7375–9.

Fioravanti, K.J. & German, R.M., 1988. Corrosion and tarnishing characteristics of low content dental casting alloys. *Gold Bulletin* 21, 99–110.

Fitton J.L., Meeks N.D. & Joyner, L., 2009. The Aigina treasure: catalogue and technical report, in *The Aigina Treasure, Aegean Bronze Age Jewellery and a Mystery Revisited*, ed. J.L. Fitton. London: The Trustees of the British Museum, 17–31.

Fontenay, E., 1887. *Les bijoux anciens et modernes*. Paris: Maison Quantin.

Forty, A.J., 1981. Micromorphological studies of the corrosion of gold alloys. *Gold Bulletin* 14, 25–35.

Frantz, J.H. & Schorsch, D., 1990. Egyptian Red Gold. *Archeomaterials* 4, 133–52.

Freestone, I., Meeks, N., Sax, M. & Higgitt, C. 2007. The Lycurgus Cup - A Roman nanotechnology. *Gold Bulletin* 40, 270–7.

Freeth, T., Bitsakis, Y., Moussas, X., Seiradakis, J.H., Tselikas, A., Mangou, H., Zafeiropoulou, M., Hadland,, R., Bate, D., Ramsey, A., Allen, M., Crawley, A., Hockley, P., Malzbender, T., Gelb, D., Ambrisco, W. & Edmunds, M.G., 2006. Decoding the ancient Greek astronomical calculator known as the Antikythera Mechanism. *Nature* 444(30), 587–91.

Friel, J.J. & Lyman, C.H., 2006. X-ray Mapping in Electron-Beam Instruments. *Microscopy and Microanalysis* 12, 2–25.

Fujita, T., 2017. Hierarchical nanoporous metals as a path toward the ultimate three-dimensional functionality. *Science and Technology of Advanced Materials* 18(1), 724–40.

Gale, N. & Stos-Gale, Z. A., 1981. Ancient Egyptian Silver. *Journal of Egyptian Archaeology* 67, 103–15.

Goldstein, J.I., Newbury, D.E., Michael, J.R., Ritchie, N.W.M., Scott, J.H.J. & Joy, D.C., 2018. *Scanning Electron Microscopy and X-Ray Microanalysis*, 4th Edition. New York: Springer-Verlag.

Griesser, M., Traum, R., Mayerhofer, K.E., Piplits, K., Denk, R. & Winter, H., 2005. Brown spot corrosion on historic gold coins and medals. *Surface Engineering* 21, 385–92.

Grimwade, M.F., 2002. *Handbook on soldering and other joining techniques in gold jewellery manufacture*. London: World Gold Council.

Guerra, M.F., 2004. Fingerprinting ancient gold with proton beams of different energy. *Nuclear Instruments and Methods in Physics Research B* 226, 2004, 185–98.

Guerra, M.F., 2006. Etruscan gold jewellery pastiches of the Campana's collection revealed by scientific analysis, in *De Re Metallica*, eds. M. Cavalini & G.E. Gigante. Roma: L'Erma di Bretschneider, 103–128

Guerra, M.F., 2007. Examen et analyse de quelques bijoux de la collection Campana, in *Les bijoux de la collection Campana, de l'antique au pastiche*, eds. F. Gaultier & C. Metzger. Paris: École du Louvre, 145–77.

Guerra, M.F., 2008. An overview on the ancient goldsmith's skill and the circulation of gold in the past: the role of X-ray based techniques. *X-ray Spectrometry* 37, 317–27.

Guerra, M.F., 2018. Physicochemical approaches to gold and silver work, an overview: Searching for technologies, tracing routes, attempting to preserve. *Physical Sciences Reviews* 4(2), 1–15.

Guerra, M.F., 2021. On gold recycling. A physicochemical point of view. *Archaeometry* 64(S1), 134–49.

Guerra, M.F. & Calligaro, T., 2004. Gold traces to trace gold. *Journal of Archaeological Science* 31, 1199–1208.

Guerra, M.F. & Pagès Camagna, S., 2019. On the way to the New Kingdom. Analytical study of Queen Ahhotep's gold jewellery (17th Dynasty of Egypt). *Journal of Cultural Heritage* 36, 143–52.

Guerra, M.F. & Rehren, T., 2009. In-situ examination and analysis of the gold jewellery from the Phoenician tomb of Kition (Cyprus). *ArcheoSciences* 33, 151–8.

Guerra, M.F. & Tissot, I., 2013. The role of nuclear microprobes in the study and conservation of gold and silver cultural heritage items: an overview. *Nuclear Instruments and Methods in Physics Research B* 306, 227–31.

Guerra, M.F. & Tissot, I., 2015. Bronze Age and Iron Age gold torcs and earrings from the Iberian Atlantic façade: a non-invasive multi-analytical approach to the characterisation of the alloys and the corrosion. *X-ray spectrometry* 45(1), 5–13.

Guerra, M.F., Calligaro, T., Radtke, M., Reiche, I. & Riesemeier, H., 2005. Fingerprinting ancient gold by measuring Pt with spatially resolved high energy Sy-XRF. *Nuclear Instruments and Methods in Physics Research Section B* 240(1-2), 505–11.

Guerra, M.F., Radtke, M., Reiche, I., Riesemeier, H. & Strub, E., 2008. Analysis of trace elements in gold alloys by SR-XRF at high energy at the BAMline. *Nuclear Instruments and Methods in Physics Research B* 266(10), 2334–8.

Gusmano, G., Montanari, R., Kaciulis, S., Mezzi, A., Montesperelli, G. & Rupprecht, L., 2004a. Surface defects on collection coins of precious metals. *Surface and Interface Analysis* 36, 921–4.

Gusmano, G., Montanari, R., Kaciulis, S., Montesperelli, G. & Denk, R., 2004b. "Gold corrosion": red stain on a gold Austrian Ducat. *Applied Physics* A 79(2), 205–11.

Hacke, A.M., Carr, C., Brown, A. & Howell, D., 2003. Investigation into the nature of metal threads in a Renaissance tapestry and the cleaning of tarnished silver by UV/Ozone (UVO) treatment. *Journal of Material Science* 38, 3307–14.

Hass, G., 1955. Filmed surfaces for reflecting optics. *Journal of the Optical Society of America* 45, 945–52.

Hess, M. & Robson, S., 2010. 3D colour imaging for cultural heritage artefacts, in *Proceedings of 5th Mid-Term Symposium Close Range Image Measurement Techniques*, eds. J.P. Mills, D.M. Barber, P.E. Miller & I. Newton. International Archives of the Photogrammetry, Remote Sensing and Spatial Information Sciences 38(5), 288–92.

Hinsch, J., 2007. Mating Cameras to Microscopes in Digital Microscopy, in *Methods in Cell Biology* 81, 3rd Edition, eds. G. Sluder & D.E. Wolf. Elsevier Inc. 55–21.

Huang, X., Uffelman, E., Cossairt, O., Walton, M. & Katsaggelos, A.K., 2016. Computational Imaging for Cultural Heritage: Recent developments in spectral imaging, 3-D surface measurement, image relighting, and X-ray mapping. *IEEE Signal Processing Magazine* 33(5), 130–8.

Huang, H., Xu, G. & Liu, X., 2021. Study on the Purity of Gold Leaf in a $SO_2$ Atmosphere at Ambient Temperature. *Material* 14(9), 2425.

Ioanid, E.G., Ioanid, A., Rusu, D.E. & Doroftei, F., 2011. Surface investigation of some medieval silver coins cleaned in high-frequency cold plasma. *Journal of Cultural Heritage* 12, 220–6.

Jansen, M., Hauptmann, A., Klein, S., & Zettler, R.L., 2021. Trace Elements and Isotopes: The Origin of Gold from Ur from a Geochemical Point of View, in *Ur in the Twenty-First Century CE*, eds. G. Frame, J. Jeffers & H. Pittman. Pennsylvania: Eisenbrauns, University Park, 273–92.

Keast, V.J., Myles, T.A., Shahcheraghi, N. & Cortie, M.B., 2016. Corrosion process of triangular silver nanoparticles compared to bulk silver. *Journal of Nanoparticle Research* 18, 45–66.

Keturakis, C.J., Notis, B., Blenheim, A., Miller, A.C., Pafchek, R., Notis, M.R. & Wachs, I.E., 2016. Analysis of corrosion layers in ancient Roman silver coins with high resolution surface spectroscopic techniques. *Applied Surface Science* 376, 224–51.

Kirz, J. & Vaughan, D., 1985. *X-ray Data Booklet*. Berkeley: Lawrence Berkeley Laboratory, University of California.

Kodak, 1966. Industrial Radiography. London: Kodak Ltd.

Kovacs, R., Schlosser, S., Staub, S.P., Schmiderer, A., Pernicka, E. & Günther, D., 2009. Characterization of calibration materials for trace element analysis and fingerprint studies of gold using LA-ICP-MS. *Journal of Analytical Atomic Spectrometry* 24(4), 476–83.

Lang, J. & Middleton, A. (eds.), 2005. Radiography of Cultural Material, 2nd edition. Oxford: Butterworth-Heinemann.

Lee, H.J., Chen, Y.B. & Zhang, Z.M., 2006. Directional radiative properties of anisotropic rough silicon and gold surfaces. *International Journal of Heat and Mass Transfer* 49(23), 4482–95.

Lee, J.M., Yu, J. & Koh, Y., 2003. Experimental study on the effect of wavelength in the laser cleaning of silver threads. *Journal of Cultural Heritage* 4, 157–61.

Lemasson, Q., Moignard, B., Pacheco, C., Pichon, L. & Guerra, M.F., 2015. Fast mapping of gold jewellery from ancient Egypt with PIXE: Searching for hard-solders and PGE inclusions. *Talanta* 143, 279–86.

Liang, C., Yang, C. & Huang, N., 2011. Investigating the tarnish and corrosion mechanisms of Chinese gold coins. *Surface and Interface Analysis* 43, 763–9.

Lilyquist, C., 1993. Granulation and Glass: Chronological and Stylistic Investigations at Selected Sites, c. 2500–1400 BCE. *Bulletin of the American Schools of Oriental Research* 290/291, 29–94.

Lilyquist, C., 1994. The Dilbat hoard. *The Metropolitan Museum Journal* 29, 5–36.

Lilyquist, C., 2003. *The tomb of the three foreign wives of Tuthmosis III*. New York: The Metropolitan Museum of Art.

Lu, T., Zhang, J., Lan, Y., Ma, Y., Chen, H., Ke, J. Wu, Z. & Tang, M., 2015. Characterization of tarnish spots in Chinese high-purity gold jewelry. *Gems & Gemology* 51, 410–18.

Lucas, A., 1926. *Ancient Egyptian materials and industries*. London: Edward Arnold Publishers Ltd.

MacDonald, L.W., 2010. The limits of resolution, in *Proceedings of the 2010 international conference on Electronic Visualisation and the Arts*, eds. A. Seal, J.P. Bowen, J.P. Bowen & K. Ng. Swindon: BCS Learning & Development Ltd., 149–56.

MacDonald, L.W., 2011. Choosing optimal wavelengths for colour laser scanners, in *Nineteenth Color and Imaging Conference Proceedings*. San José, California: Society for Imaging Science and Technology, 357–62.

MacDonald, L.W., 2014. Colour and directionality in surface reflectance. *Proceedings of Artificial Intelligence and the Simulation of Behaviour*. London: Society for the Study of Artificial Intelligence and the Simulation of Behaviour.

MacDonald, L.W., 2015. Surface reconstruction from photometric normals with reference height measurements, in *Optics for Arts, Architecture, and Archaeology V*, eds. L. Pezzati & P. Targowski. SPIE Conference Proceedings 9527. The International Society for Optical Engineering, Article 952706.

MacDonald, L.W. & Robson, S., 2010. Polynomial texture mapping and 3D representations, in *Proceedings of 5th Mid-Term Symposium Close Range Image Measurement Techniques*, eds. J.P. Mills, D.M. Barber, P.E. Miller & I. Newton. International Archives of the Photogrammetry, Remote Sensing and Spatial Information Sciences 38(5), 422–7.

MacDonald, L.W., Hosseininaveh Ahmadabadian, A. & Robson, S., 2015. Determining the coordinates of lamps in an illumination dome, in V*ideometrics, Range Imaging, and Applications XIII*, eds. F. Remondino & M.R. Shortis. SPIE Conference Proceedings 9528. The International Society for Optical Engineering, Article 95280I.

MacDonald, L.W., Guerra, M.F., Pillay, R., Hess, M., Quirke, S., Robson, S. & Hosseininaveh Ahmadabadian, A., 2014. Practice-based comparison of imaging methods for visualization of toolmarks on an Egyptian scarab, in *Image and Signal Processing*, eds. A. Elmoataz, O. Lezoray, F. Nouboud & D. Mammass. Lecture Notes in Computer Science 8509. Cham, Switzerland: Springer, 239–46.

Martinón-Torres, M., Valcárcel Rojas, R., Sáenz Samper, J. & Guerra, M.F., 2012. Metallic encounters in Cuba: The technology, exchange and meaning of metals before and after Columbus. *Journal of Anthropological Archaeology* 31, 439–54.

Maryon, H., 1941. Archæology and Metallurgy. I. Welding and Soldering, *MAN* 41(85), 118–24.

Maxwell, J.A., Campbell, J.L. & Teesdale, W.J., 1989. The Guelph PIXE software. *Nuclear Instruments and Methods in Physics Research B* 43, 218–30.

McGovern, P.E., 1985. *Late Bronze Age Palestinian pendants. Innovation in a Cosmopolitan Age*. JSTO/ASOR Monograph Series 1. Sheffield: JSOT Press.

Meeks, N.D., 1998. Pre-hispanic goldwork in the British Museum: some recent technological studies. *Boletín Museo del Oro* 44-45, 107–37.

Meeks, N.D., 2000. Scanning Electron Microscopy of the Refractory Remains and the Gold, in *King Croesus' Gold*, eds. A. Ramage & P. Craddock. London: British Museum Press, 99–156.

Meeks, N.D. & Tite, M.S., 1980. The analysis of platinum-group element inclusions in gold antiquities. *Journal of Archaeological Science* 7(3), 267–75.

Meeks, N., Cartwright, C., Meek, A. & Mongiatti, A. (eds.), 2012. *Historical technology, materials and conservation. SEM and Microanalysis*. London: Archetype Publications and The British Museum.

Meidinger, N., Andritschke, R., Hartmann, R., Herrmann, S., Holl, P., Lutz, G. & Strueder, L., 2006. pnCCD for photon detection from near-infrared to X-rays. *Nuclear Instruments and Methods in Physics Research A* 565(1), 251–7.

Merriman, C.C., Bahr, D.F. & Norton, M.G., 2005. Environmentally induced failure of gold jewelry alloys. *Gold Bulletin* 38, 113–19.

Miniaci, G., La Niece, S., Guerra, M.F. & Hacke, M., 2013. Analytical study of the first royal Egyptian heart-scarab, attributed to a Seventeenth Dynasty king, Sobekemsaf. *British Museum Technical Research Bulletin* 7, 53–60.

Morigi, M.P., Casali, F., Bettuzzi, M., Brancaccio, R. & D'Errico, V., 2010. Application of X-ray Computed Tomography to Cultural Heritage diagnostics. *Applied Physics A* 10(3), 653–61.

Negbi, O., 1970. *The hoards of goldwork from Tell el-Ajjul*. Studies in Mediterranean Archaeology. Göteborg: Södra, Vägen 61.

Nestler, G. & Formigli, E., 2004. G*ranulazione etrusca un'antica arte orafa*. Sienna: Nuova imagine.

Northover, S.M. & Northover, J.P., 2012. Applications of Electron Backscatter Diffraction (EBSD) in Archaeology, in *Historical technology, materials and conservation. SEM and Microanalysis*, eds. N. Meeks, C. Cartwright, A. Meek & A. Mongiatti. London: Archetype Publications and The British Museum, 76–85.

Oddy, A., 1977. The production of gold wire in Antiquity. Hand-making methods before the introduction of the draw-plate. *Gold Bulletin* 3(10), 79–87.

Oddy, A., 2004. The manufacture of wire since the Bronze Age: a technological investigation using the microscope, in *Physics methods in archaeometry*, eds. M. Martini, M. Milazzo & M. Piacentini. Amsterdam: IOS Press, 257–67.

Ogden, J.M., 1977. Platinum group metal inclusions in Ancient gold artifacts. *Journal of the Historical Metallurgy Society* 11(2), 53–70.

Olsen, S.L., 1988. Applications of Scanning Electron Microscopy in Archaeology. *Advances in Electronics and Electron Physics* 71, 357–80.

Ordavo, I., Ihle, S., Arkadiev, V., Scharf, O., Soltau, H., Bjeoumikhov, A., Bjeoumikhova, S., Buzanich, G., Gubzhokov, R., Gunther, A., Hartmann, R., Holl, P., Kimmel, N., Kuhbacher, M., Lang, M., Langhoff, N., Liebel, A., Radtke, M., Reinholz, U., Riesemeier, H., Schaller, G., Schopper, F., Struder, L., Thamm, C. & Wedell, R., 2011. A new pnCCD-based color X-ray camera for fast spatial and energy-resolved measurements. *Nuclear Instruments & Methods in Physics Research Section A* 654(1), 250–7.

Palomar, T., Barat, B.R., García, E. & Cano, E., 2016. A comparative study of cleaning methods for tarnished silver. *Journal of Cultural Heritage* 17, 20–6.

Paris, O., Li, C., Siegel, S., Weseloh, G., Emmerling, F., Riesemeier, H., Erko, A. & Fratzl, P., 2007. A new experimental station for simultaneous X-ray microbeam scanning for small- and wide-angle scattering and fluorescence at BESSY II. *Journal of Applied Crystallography* 40, S466–S470.

Parrini, P., Formigli, E. & Mello, E., 1982. Etruscan Granulation: Analysis of Orientalizing Jewelry from Marsiliana d'Albegna. *American Journal of Archaeology* 86(1), 118–21.

Perea, A., García Vuelta, O. & Fernández Freire, C., 2010. *El proyecto AU, estudio arqueométrico de la producción de oro en la Península Ibérica*. Madrid: CSIC.

Pérez-Arantegui, J. & Larrea, A., 2015. Electron backscattering diffraction as a complementary analytical approach to the microstructural characterization of ancient materials by electron microscopy. *Trends in Analytical Chemistry* 72, 193–201.

Petrie, W.M.F., 1909. *Qurneh*. London: British School of Archaeology in Egypt.

Petrie, W.F., 1931-4. *Ancient Gaza I to IV*. British School of Archaeology in Egypt. London: Quaritch.

Petrie, W.F., 1952. *City of Shepherd Kings. Ancient Gaza V*. British School of Archaeology in Egypt. London: Quaritch.

Petrie, W.M.F. & Quibell, J.E., 1896. *Naqada and Ballas*. London: B. Quaritch ed.

Pichon, L., Moignard, B., Lemasson, Q., Pacheco C. & Walter, P., 2014. Development of a multi-detector and a systematic imaging system on the AGLAE external beam. *Nuclear Instruments and Methods in Physics Research B* 318, 27–31

Pichon, L., Calligaro, T., Lemasson, Q., Moignard, B. & Pacheco, C., 2015. Programs for visualization, handling and quantification of PIXE maps at the AGLAE facility. *Nuclear Instruments and Methods in Physics Research B* 363, 48–54.

Platz-Horster, G. & Tietz, H.U., 1995. Sulla granulazione degli etruschi, in *Preziosi in oro, avorio, osso e corno*, ed. E. Formigli. Siena: Nuova Imagine, 56–62.

Politis, T., 2001. Gold and Granulation: Exploring the Social Implications of a Prestige Technology in the Bronze Age Mediterranean, in *The social context of technological change: Egypt and the Near East, 1650–1550 BC*, ed. A.J. Shortland. Oxford: Oxbow Books, 161–94.

Politis, T., Abraham, M., Northover, P. & Grime, G., 2002. PIXE, Electron Microprobe Data, and Experimental Archaeology: Tell el-Ajjul and Pilot Studies of Gold Granulation Joining Practices in the Mediterranean Bronze Age. *Materials Research Society Symposium Proceedings* 712, II7.3.1–10.

Ponting, M., 2004. The scanning electron microscope and the archaeologist. *Physics Education* 39(2), 166–70.

Pulak, C., 2008. The Uluburun shipwreck and Late Bronze Age trade, in *Beyond Babylon. Art Trade and Diplomacy in the Second Millennium BC,* eds. J. Aruz. K. Benzel & J. M. Evans. New York / New Haven / London: The Metropolitan Museum of Art / Yale University Press, 289–310.

Radtke, M., Reinholz, U. & Gebhard, R., 2017. Synchrotron Radiation–Induced X-Ray Fluorescence (SRXRF) Analyses of the Bernstorf gold. *Archaeometry* 59(5), 891-9.

Radtke, M., Buzanich, G., Guilherme, A., Reinholz, U., Riesemeier, H., Scharf, O., Scholz, P. & Guerra, M.F., 2016. Double Dispersive X-Ray Fluorescence (D2XRF) based on an Energy Dispersive pnCCD detector for the detection of platinum in gold. *Microchemical Journal* 125, 56–61.

Radtke, M., Reiche, I., Reinholz, U., Riesemeier, H. & Guerra, M.F., 2013. Beyond the Great Wall: Gold of the Silk Roads and the First Empire of the Steppes. *Analytical Chemistry* 85(3), 1650–6.

Randin, J.P., Ramoni, P. & Renaud, J.P., 1992. Tarnishing of AuAgCu alloys. Effect of the composition. *Materials and Corrosion* 43, 115–23.

Rapson, W.S., 1996. Tarnish resistance, corrosion and stress corrosion cracking of gold alloys. *Gold Bulletin* 29, 61–9.

Riesemeier, H., Ecker, K., Görner, W., Müller, B.R, Radtke, M. & Krumrey, M., 2005. Layout and first XRF Applications of the BAMline at BESSY II. *X-Ray Spectrometry* 34(2), 160–3.

Rifai, M.M. & El Hadidi, N.M., 2010. Investigation and analysis of three gilded wood samples from the tomb of Tutankhamun, in *Decorated Surfaces on Ancient Egyptian Objects, Technology, Deterioration and Conservation*, eds. J. Dawson, C. Rozeik & M.M. Wright. London: Archetype Publications Ltd., 16–24.

Saeger, K.E. & Rodies, J., 1977. The colour of gold and its alloys. *Gold Bulletin* 10(1), 10–14.

Saleem, S.N. & Hawass, Z., 2014. Multidetector Computed Tomographic study of amulets, jewelry, and other foreign objects in Royal Egyptian Mummies dated from the 18th to 20th Dynasties. *Journal of Computer Assisted Tomography* 38(2), 153–8.

Salem, Y., 2017. The influence of gaseous pollutants on silver artifacts tarnishing. *Open Journal of Air Pollution* 6, 135–48.

Sarkar, N.K., Fuys, R.A. & Stanford, J.W. 1979. The chloride corrosion of low-gold casting alloys. *Journal of Dental Research* 58, 568–75.

Sawada, H., Borisenko, K.B., Shima, M., Ikita, K., Hashiguchi, H., Onishi, I., Okunishi, E. & Kirkland, A.I., 2019. Corrosion of Gold by a Nanoscale Gold and Copper Beltlike Structure. *Journal of Physical Chemistry C* 123(32), 19920–6.

Scharf, O., Ihle, S., Ordavo, I., Arkadiev, V., Bjeoumikhov, A., Bjeoumikhova, S., Buzanich, G., Gubzhokov, R., Guenther, A., Hartmann, R., Kuehbacher, M., Lang, M., Langhoff, N., Liebel, A., Radtke, M., Reinholz, U., Riesemeier, H., Soltau, H., Strueder, L., Thuenemann, A.F. & Wedell, R., 2011. Compact pnCCD-Based X-ray Camera with High Spatial and Energy Resolution: A Color X-ray Camera. *Analytical Chemistry* 83(7), 2532–8.

Schlosser, S., Reinecke, A., Schwab, R., Pernicka, E., Sonetra, S. & Laychour, V., 2012. Early Cambodian gold and silver from Prohear: composition, trace elements and gilding. *Journal of Archaeological Science* 39(9), 2877–87.

Schorsch, D., 1995. The Gold and Silver Necklaces of Wah. A Technical Study of an Unusual Metallurgical Joining

Method, in *Conservation in ancient Egyptian collections*, eds. C. Brown, F. Macalister & M. Wright. London: Archetype Publications, 127–35.

Schreiner, M., Melcher, M. & Uhlir, K., 2007. Scanning electron microscopy and energy dispersive analysis: applications in the field of cultural heritage. *Analytical and Bioanalytical Chemistry* 387, 737–47.

Sciau, Ph., 2016. Transmission Electron Microscopy: Emerging Investigations for Cultural Heritage Materials, in *Advances in Imaging and Electron Physics* 198, ed. P.W. Hawkes. Elsevier Inc., 43–67.

Scrivano, S., Ruberto, C., Gómez-Tubío, B., Mazzinghi, A., Ortega-Feliu, I., Ager, F.J., Laclavetine, K., Giuntini, L. & Respaldiza, M.A., 2017. In-situ non-destructive analysis of Etruscan gold jewels with the micro-XRF transportable spectrometer from CAN. *Journal of Archaeological Science: Reports* 16,185–93.

Seipel, W., 2001. *Gold der Pharaonen*. Kunsthistorschen Museum. Viena: Skira ed.

Shafer, S.A., 1985. Using color to separate reflection components. *Color Research & Application* 10(4), 210–18.

Siano, S. & Salimbeni, R., 2010. Advances in laser cleaning of artwork and objects of historical interest: the optimized pulse duration. *Accounts of Chemical Research* 43(6), 739–50.

Silverman, D., 1997. *Searching for Ancient Egypt.* Dallas: Dallas Museum of Art, Cornell University Press.

Snape, S., 1987. *Mortuary Assemblages from Abydos I*. PhD Dissertation, University of Liverpool.

Sokaras, D., Mueller, M., Kolbe, M., Beckhoff, B., Zarkadas, C. & Karydas, A.G., 2010. Resonant Raman scattering of polarized and unpolarized X-ray radiation from Mg, Al, and Si. *Physical Review A* 81(1), 012703.

Solé, V.A., Papillon, E., Cotte, M., Walter, P. & Susini, J., 2007. A multiplatform code for the analysis of energy-dispersive X-ray fluorescence spectra. *Spectrochimica Acta Part B* 62, 63–8.

Standish, C., Dhuime, B., Hawkesworth, C. & Pike, A., 2015. A Non-local Source of Irish Chalcolithic and Early Bronze Age Gold. *Proceedings of the Prehistoric Society* 81, 149–77.

Stokes, D.J., 2008. *Principles and Practice of Variable Pressure/ Environmental Scanning Electron Microscopy (VP-ESEM).* John Wiley & Sons, Ltd.

Stokes, D.J., 2012. Environmental scanning electron microscopy for biology and polymer science, *Microscopy and Analysis*, 25th Anniversary Issue, 67–71.

Tate, J., Eremin, K., Troalen, L.G., Guerra, M.F., Goring, E. & Manley, W.P., 2009. The 17th dynasty gold necklace from Qurneh, Egypt. *ArcheoSciences* 33, 121–8.

Thiaudière, C., 2005. *Étude technique et typologique de la bijouterie ptolémaïque et romaine d'Égypte*. PhD Dissertation, Université de Limoges, section Histoire ancienne et archéologie.

Tissot, I., Correia, J., Monteiro, O.C., Barreiros, M.A. & Guerra, M.F., 2019. When gold stops glittering: corrosion mechanisms of René Lalique's Art Nouveau jewellery. *Journal of Analytical Atomic Spectrometry* 34, 1216–22.

Tissot, I., Monteiro, O.C., Barreiros, M.A., Correira, J. & Guerra, M.F., 2016. Corrosion of silver alloys in sulphide environments: a multianalytical approach for surface characterisation. *RSC Advances* 6, 51856–63.

Tissot, I., Monteiro, O.C., Barreiros, MA., Correira, J. & Guerra, M.F., 2017. The influence of the constituent elements on the corrosion mechanisms of silver alloys in sulphide environments: the case of sterling silver. *RSC Advances* 7, 28564–72.

Tissot, I., Tissot, M. & Guerra, M.F., 2014. Atmospheric corrosion in museum context – the case of the treasure room from the National Archaeology Museum, Lisbon. *Corrosão e Protecção de Materiais* 4, 73–7.

Tissot, I., Tissot, M., Manso, M., Alves, L.C., Barreiros, M.A., Marcelo, T., Carvalho, M.L., Corregidor, V. & Guerra, M.F., 2013. The earrings of Pancas Treasure: Analytical study by X-ray based techniques – A first approach. *Nuclear Instruments and Methods in Physics Research B* 306, 236–40.

Tissot, I., Troalen, L.G., Manso, M., Ponting, M., Radtke, M., Reinholz, U., Barreiros, M.A., Shaw, I., Carvalho, M.L. & Guerra, M.F., 2015. A multi-analytical approach to gold in Ancient Egypt: Studies on provenance and corrosion. *Spectrochimica Acta Part B* 108, 75–82.

Troalen, L.G. & Guerra, M.F., 2016. Gold from the tomb of Scribe Beri: a comparative analytical approach to the New Kingdom gold grave goods from Riqqa (Egypt). *Applied Physics A* 122, 210–16.

Troalen, L., Guerra, M.F., Tate, J. & Manley, W.P., 2009. Technological study of gold jewellery pieces dated from Middle Kingdom to New Kingdom in Egypt. *ArcheoSciences* 33, 111–19.

Troalen, L.G., Cox, D., Skinner, T., Ramsey, A. & Bate, D., 2010. Three-dimensional Computed Tomography X-Radiographic investigation of a 17th century watch from the wreck of the Swan, off Duart Point, Mull, Scotland. *International Journal of Nautical Archaeology* 39, 165–171.

Troalen, L., Guerra, M.F., Maitland, M., Ponting, M. & Price, C., 2019, Analytical study of the Middle Kingdom group of gold jewellery from tomb 124 at Riqqa, Egypt. *X-ray Spectrometry* 48(6), 586–96.

Troalen, L.G., Tissot, I., Maitland, M. & Guerra, M.F., 2016. Jewellery of a young Egyptian girl: Middle Kingdom goldwork from Haraga tomb 72. *Historical Metallurgy* 49, 75–86.

Troalen, L.G., Guerra, M.F. & Tate, J., 2014. Goldwork in Ancient Egypt. Workshop practices at Qurneh in the 2nd Intermediate Period. *Journal of Archaeological Sciences* 50, 219–26.

Tufnell, O., 1983. Some Gold Bird Ornaments Falcon or Wryneck? *Anatolian Studies* 33, 57–66.

Ul-Hamid, A., 2018. *A Beginners' Guide to Scanning Electron Microscopy*. Switzerland: Springer Nature.

Vassilou, P., Novakovic, J., Ingo, G.M. & de Caro, T., 2009. Corrosion of ancient silver alloys, in *Corrosion control in service of society, 17th International Corrosion Congress*. Houston: NACE International Inc., 2879.

Viguerie, L. de, Duran, A., Bouquillon, A., Solé, V.A., Castaing, J. & Walter, P., 2009. Quantitative X-ray fluorescence analysis of an Egyptian faience pendant and comparison with PIXE. *Analytical and Bioanalytical Chemistry* 395, 2219–25.

Wanhill, R.J.H., Steijaart, J.P.H.M., Leenheer, R. & Koens, J.F.W., 1998. Damage assessment and preservation of an Egyptian silver vase (300–200 BC). *Archaeometry* 40, 123–37.

Wanhill, R.J.H., 2011. Case histories of ancient silver embrittlement. *Journal of Failure Analysis and Prevention* 11, 178–85.

Weissmüller, J., Newman, R.C., Jin, H.J., Hodge, A.M. & Kysar, J.W., 2009. Nanoporous metals by alloy corrosion: formation and mechanical properties. *Materials Research Society Bulletin* 34(8), 577–86.

Wharton, G., Maish, S.L. & Ginell, W.S., 1990. A comparative study of silver cleaning abrasives. *Journal of the American Institute for Conservation* 29, 13–31.

Williams, D.B. & Carter, C.B., 2009. *Transmission Electron Microscopy. A Textbook for Materials Science*, 2nd edition. Springer Science, Business Media.

Wolf, D.E., 2007. The Optics of Microscope Image Formation in Digital Microscopy, in *Methods in Cell Biology* 81, 3rd edition, eds. G. Sluder & D.E. Wolf. Elsevier Inc., 12–42.

Wu, Q., Watts, B., Döbeli, M., Müller, J., Butz, B., Lombardo, T., Schmidt-Ott, K., Fink, R., Nolting, F. & Ganz, D., 2021. Medieval nanotechnology: Thickness determination of Zwischgold samples. *Journal of Cultural Heritage* 49, 211–21.

Yang, C., Liang, C. & Wang, P., 2007. Investigation of the tarnish on the surface of a panda gold coin. *Rare Metals* 26, 6–73.